Letter

Magic transfer in quantum spin chains

Antonio Palamara [1,2,*] Chad Nelmes [3,4,*] Enrico C. Domanti [5] and Francesco Perciavalle [1,2,†]

[1] *Dipartimento di Fisica, Università della Calabria, 87036 Arcavacata di Rende (CS), Italy*
[2] *Gruppo Collegato di Cosenza, INFN, 87036 Arcavacata di Rende, Cosenza, Calabria, Italy*
[3] *School of Physics, Engineering and Technology, University of York, York YO10 5DD, United Kingdom*
[4] *York Centre for Quantum Technologies, University of York, York YO10 5DD, United Kingdom*
[5] *Instituto de Física Teórica, UAM-CSIC, Universidad Autonoma de Madrid, Cantoblanco, 28049 Madrid, Spain*

(Received 19 June 2026; revised 13 September 2026; accepted 27 October 2026; published 5 November 2026)

Quantum communication protocols based on spin chains have been extensively studied, yet their ability to transmit nonstabilizer resources has not been systematically addressed. We investigate the transport of quantum magic in spin chains through the natural dynamics of systems initialized in nonstabilizer states, and quantify the transported resource via the stabilizer norm. We analyze three experimentally feasible state-transfer protocols, ranging from noisy to (quasi)perfect transfer, including one realizable in trapped-ion platforms. We find that the geometry of the injected state strongly influences transport: States in the lower Bloch hemisphere achieve higher transfer quality, whereas states in the upper hemisphere give rise to an efficient magic transport only beyond a threshold value of the parameter controlling the tendency toward perfect transfer. These features are robust across all protocols and identify the Hamiltonian and state properties that favor high-quality transfer. Moreover, we identify a parameter region, relevant to the initial state preparation, in which the transported magic exceeds the initial encoding, indicating that such spin systems can act as magic-amplification channels. Our results establish the conditions for efficient transport of nonstabilizer resources and demonstrate quantum magic as a sensitive probe of quantum transport beyond population dynamics.

DOI: 10.1103/mq4t-pnby

Introduction. Quantum state transfer (QST) is a well-established field of quantum information processing, motivated by the need to reliably transmit quantum information across scalable quantum architectures [1–12]. Over the past two decades, extensive theoretical and experimental work has demonstrated that engineered spin chains can act as efficient quantum communication channels when the Hamiltonian parameters are appropriately tuned, enabling high-fidelity transport of localized single-excitation states as well as entanglement generation/distribution [13–16].

The performance of QST protocols is conventionally characterized by the average transfer fidelity, which quantifies how accurately an arbitrary input state is reconstructed at the receiving

*These authors contributed equally to this work.
†Contact author: fraperciavalle97@gmail.com

Published by the American Physical Society under the terms of the Creative Commons Attribution 4.0 International license. Further distribution of this work must maintain attribution to the author(s) and the published article's title, journal citation, and DOI.

site. However, fidelity alone does not capture the transport of specific quantum resources. Of particular interest is nonstabilizerness (or magic), which is a fundamental resource for universal fault-tolerant quantum computation [17–23]. Motivated by its central role in quantum information processing, the generation, dynamics, and resilience of magic in many-body systems have recently attracted significant attention [20,24–44]. Yet, despite the extensive use of spin chains as quantum communication channels and paradigmatic platforms for perfect state transfer (PST), their ability to transport magic remains unexplored. This raises a fundamental question: How is magic transmitted through quantum spin networks away from the ideal PST regime? In particular, are some magic states more robust under transport than others, and is the underlying mechanism governing magic transfer nontrivial? Here, we address these questions by investigating magic transfer across a broad class of state-transfer protocols, ranging from ideal PST architectures to experimentally relevant imperfect-transfer regimes.

We investigate the propagation of magic encoded in injected T states, canonical single-qubit magic states enabling universal fault-tolerant quantum computation [17], through quantum spin chains acting as quantum buses, tuned away from perfect and quasiperfect state-transfer protocols. Considering three interpolation schemes connecting PST, quasiperfect state transfer (QPST), homogeneous, and long-range hopping models [2,4,45–49], we show that magic transport is governed by the geometry of quantum state space, exhibiting distinct regimes of suppression and robust propagation. Our findings further demonstrate that, depending on the initial state preparation and tuning parameters, the nonstabilizerness of the extracted state can exceed that of the initially encoded state. This reveals a novel class of spin chain quantum buses that, beyond faithfully routing information, intrinsically act as resource-amplification channels for quantum magic.

Model and methods. We aim to investigate the transfer of nonstabilizerness across a quantum spin chain composed of L qubits and described by a time-independent Hamiltonian $\hat{H}$ by analyzing its robustness under different state-transfer protocols, depending on whether the system operates close to known PST [2]/QPST [4] schemes or away from them. The protocol consists of injecting a nonstabilizer state $|\psi(0)\rangle$ at one edge of a quantum spin network, such that the initial global state is given by $|\Psi(0)\rangle = |\psi(0)\rangle \otimes |\downarrow, \ldots, \downarrow\rangle$, where all the remaining spins are initialized in the fully polarized state. The system then undergoes unitary evolution according to $|\Psi(t)\rangle = e^{-i\hat{H}t}\,|\Psi(0)\rangle$, with $\hbar = 1$. To characterize the transport of magic through the chain, we analyze the nonstabilizerness of the reduced state at each site, $\rho^{(j)}(t) = \mathrm{Tr}_{\{1,\ldots,L\}\setminus j}[|\Psi(t)\rangle\langle\Psi(t)|]$, with particular emphasis on the magic transferred to the opposite edge, described by the reduced state $\rho^{(L)}(t)$.

For single-qubit states, nonstabilizerness can be efficiently probed through the stabilizer norm (SN) [18,20,29], defined as $\mathcal{D}(\rho) = \frac{1}{2}(1 + |x| + |y| + |z|)$, where (x, y, z) are the components of the Bloch vector associated with the state ρ. The SN is not a magic monotone [50] but provides a strong necessary and sufficient condition for single-qubit states. Pure stabilizer states satisfy $\mathcal{D}(|\psi_{\mathrm{st}}\rangle\langle\psi_{\mathrm{st}}|) = 1$, while all mixed stabilizer states obey $\mathcal{D}(\rho_{\mathrm{st}}) \leqslant 1$, which we define as the polytope bound. Therefore, the condition $\mathcal{D}(\rho) > 1$ provides a necessary and sufficient criterion for nonstabilizerness. This makes the SN a faithful and particularly powerful characterization of nonstabilizerness for single-qubit states, as it provides a necessary and sufficient condition for a state to lie outside the stabilizer set. This property, however, is specific to the single-qubit case and does not generally extend to larger systems, where nonstabilizer states with $\mathcal{D}(\rho) < 1$ can exist [20,29]. For the single-qubit states considered here, the above criterion has a direct geometric interpretation in terms of the Bloch sphere: Stabilizer states occupy a distinguished region of the Bloch sphere bounded by an octahedron whose six vertices correspond to the Pauli eigenstates located at $(\pm1, 0, 0)$, $(0, \pm1, 0)$, and $(0, 0, \pm1)$. Any state inside or on the surface of this octahedron is a stabilizer state, whereas states lying outside of it are nonstabilizer (magic) states. The SN is directly tied to the defining inequality of the octahedron, becoming larger than unity precisely when the state leaves the stabilizer region.

We choose the state $|\psi(0)\rangle = |T\rangle$, where $|T\rangle$ denotes a pure single-qubit state whose Bloch vector has components $\frac{1}{\sqrt{3}}(\pm1, \pm1, \pm1)$, corresponding to maximal SN $\mathcal{D}(|T\rangle\langle T|) = \frac{1+\sqrt{3}}{2}$. A

representative choice is $|T_+\rangle = \cos\beta\,|\uparrow\rangle + e^{i\pi/4}\sin\beta\,|\downarrow\rangle$, where the parameter β is defined by $\cos(2\beta) = \frac{1}{\sqrt{3}}$. The Bloch vector of the initial state $\mathbf{r}_0^{(1)} = [x_0^{(1)}, y_0^{(1)}, z_0^{(1)}]$ is propagated through the chain dynamics to the Bloch vector $\mathbf{r}_t^{(j)} = [x_t^{(j)}, y_t^{(j)}, z_t^{(j)}]$ of the reduced density matrix at site j, according to the affine transformation

$$\mathbf{r}_t^{(j)} = \mathbf{M}_t^{(j)}\,\mathbf{r}_0^{(1)} + \mathbf{c}_t^{(j)}, \tag{1}$$

where $\mathbf{M}_t^{(j)}$ and $\mathbf{c}_t^{(j)}$ are, respectively, a matrix and a vector that depend on the single-excitation transition amplitude $f_j(t) = \langle j|e^{-i\hat{H}t}|1\rangle$ (see the Supplemental Material [51]). Here, $|j\rangle = |\downarrow,\ldots,\uparrow_j,\ldots,\downarrow\rangle$ denotes the single-excitation state localized at site j. This affine mapping directly connects the initial local Bloch vector to its time-evolved counterpart at any site j, thereby enabling a transparent description of the transport of local quantum features across the chain. In particular, it allows for a direct evaluation of the on-site SN, $\mathcal{D}(\rho^{(j)}(t)) = \frac{1}{2}(1 + |x_t^{(j)}| + |y_t^{(j)}| + |z_t^{(j)}|)$, which we use to track propagation of nonstabilizerness along the spin chain. Finally, we note that the time-evolved Bloch components can equivalently be obtained as expectation values of local Pauli operators at site j, i.e., $x_t^{(j)} = \langle\hat{\sigma}_j^x(t)\rangle$, $y_t^{(j)} = \langle\hat{\sigma}_j^y(t)\rangle$, and $z_t^{(j)} = \langle\hat{\sigma}_j^z(t)\rangle$, establishing a direct connection between the transfer matrix description and experimentally accessible observables.

The magic transfer is studied within the zero- and single-excitation sectors of a quantum spin network governed by the XX Hamiltonian

$$\hat{H} = \sum_{i,j} J_{ij}(\hat{\sigma}_i^+\hat{\sigma}_j^- + \text{H.c.}), \tag{2}$$

where $\hat{\sigma}_j^\pm$ denote spin-raising and spin-lowering operators acting on site j. We focus on one-dimensional spin chains and consider three state-transfer protocols that continuously connect imperfect to high-fidelity transfer.

Protocol A interpolates between a homogeneous nearest-neighbor chain and the PST chain of Ref. [2] through couplings $J_{ij} = J_j^A\delta_{j,j+1}$, with $J_j^A = (1-\alpha)J + \alpha\,a_j$, where $\alpha \in [0,1]$ and $a_j = (2J/L)\sqrt{j(L-j)}$. *Protocol B* similarly interpolates between homogeneous and ballistic transfer [4], with nearest-neighbor couplings $J_{ij} = J_j^B\delta_{j,j+1}$, with $J_j^B = (1-\alpha)J + \alpha\,b_j$. Here, $b_1 = b_{L-1} = \mu$, $b_2 = b_{L-2} = \nu$, and $b_j = J$ otherwise, yielding near-unit transfer fidelity through engineering only the boundary couplings. *Protocol C* is motivated by programmable quantum simulators based on trapped ions and Rydberg-atom arrays, where interactions naturally decay as a power law [45–49,52]. We consider couplings $J_{ij} = J/d_{ij}^\lambda$, where λ controls the interaction range. The qubit positions are chosen such that $d_{j,j+1} = [2L/(\sqrt{j(L-j)})]^{1/\lambda}$, with $d_{ij} = |x_i - x_j|$. In the limit $\lambda \to \infty$, long-range couplings are suppressed and the resulting nearest-neighbor couplings approach the PST profile. In all the protocols, we consider periodic boundary conditions.

Magic transfer. We find that the nonstabilizerness dynamics is determined by the hemisphere of the initial Bloch vector, $z = \pm 1/\sqrt{3}$. All four T states within a given hemisphere exhibit identical SN dynamics [51]. We therefore focus on two representative states, $|T_+\rangle$ and $|T_-\rangle$, with Bloch vectors $\frac{1}{\sqrt{3}}(1,1,1)$ and $\frac{1}{\sqrt{3}}(1,1,-1)$, respectively (Fig. 1). As shown below, the two hemispheres display markedly different transport behavior.

Figure 2 shows the SN dynamics for systems evolving under the Protocol A Hamiltonian starting from injected T states in the upper ($|T_+\rangle$) and lower ($|T_-\rangle$) hemispheres of the Bloch sphere. For initial states in the upper hemisphere, $\mathcal{D}(\rho^{(j)}(t))$ remains comparatively small and can even temporarily drop below unity, signaling that the local Bloch vectors enter the stabilizer polytope during the evolution. Moreover, the relatively small magnitude of the SN indicates that the state at the last site hardly approaches a genuine T-like structure. Conversely, when the injected state lies in the lower hemisphere, the SN remains systematically larger, showing that the local Bloch vectors stay outside the stabilizer polytope and can approach states with a much stronger T-state character.

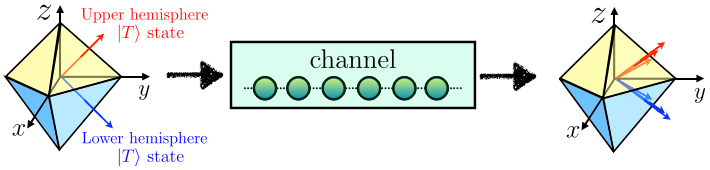


FIG. 1. Pictorial representation of the protocol: $|T\rangle$ states with maximum SN are injected at one edge of a quantum channel modeled as a spin chain and transferred to the opposite edge. The channel continuously interpolates between a perfect state-transfer regime and an imperfect-transfer regime. The transport of magic depends on the Bloch hemisphere to which the initial state belongs.

The insets in Fig. 2 (top panels) show the time evolution of $\mathcal{D}(\rho^{(L)}(t))$, highlighting clear qualitative differences between the four cases. We first consider the $\alpha = 0$ regime [Figs. 2(a) and 2(c)], where reflection times correspond to boundary scattering events of the propagating wave packets. For the initial state $|T_+\rangle$, the SN exhibits only modest growth, reaching $\mathcal{D}(\rho^{(L)}) \approx 1.11$ at the first reflection and remaining within a narrow quasiperiodic window thereafter. In contrast, for $|T_-\rangle$ it reaches a significantly larger value, $\mathcal{D}(\rho^{(L)}) \approx 1.25$, already at the first reflection, before decreasing at later times. In the PST limit $\alpha = 1$ [Figs. 2(b) and 2(d)] $\mathcal{D}(\rho^{(L)}(t))$ becomes strictly periodic and repeatedly attains its maximal value, reflecting perfect revivals. Nevertheless, the two initial states display distinct trajectories: For $|T_-\rangle$, nonstabilizerness is transported to the opposite edge without crossing the stabilizer boundary, while for $|T_+\rangle$, the evolution enters the stabilizer region, as indicated by $\mathcal{D}(\rho^{(L)}(t)) < 1$, before reaching its maximum.

This behavior admits a clear geometric interpretation on the Bloch sphere [51] . The last site is initialized in the $|\downarrow\rangle$ state in the lower hemisphere and evolved toward a target $|T_\pm\rangle$ state. For target states in the lower hemisphere, the unitary dynamics connect $|\downarrow\rangle$ to the target along shorter effective trajectories that remain in regions of high nonstabilizerness, enabling efficient magic transport. In contrast, for upper-hemisphere target states the evolution follows longer paths that approach the stabilizer region, where it becomes effectively confined to low-magic sectors, thereby suppressing the transfer of nonstabilizerness.

Maximum transferable SN. Here, we quantify the maximum SN transferred between the chain edges. Since SN probes nonstabilizerness through violation of the stabilizer-polytope bound, larger transferred values indicate better preservation of magic during transport and stronger retention of T-state-like features.

We quantify the maximum transferable SN, $\mathcal{D}_{\max} = \max_{t\in[0,T]} \mathcal{D}(\rho^{(L)}(t))$, over a time window T chosen to be sufficiently long to capture multiple reflection events of the excitation. To estimate the relevant dynamical timescale, we use the PST reflection time $\tau_{\text{ref}} J = \frac{\pi L}{4}$ [2] and set the total

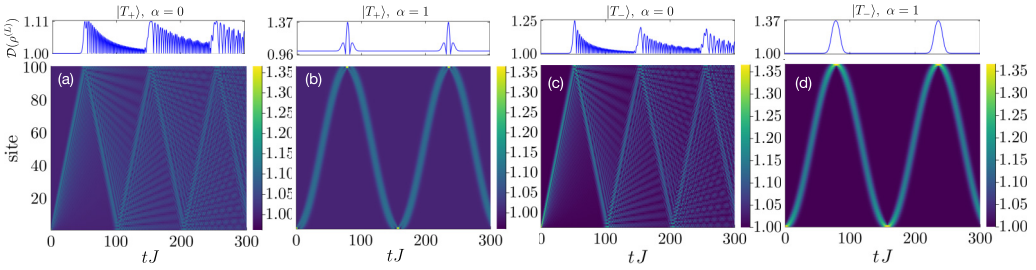


FIG. 2. On-site SN dynamics (color bar) in a spin chain described by $\hat{H}_A$ (Protocol A) composed of $L = 100$ qubits in the two asymptotic regimes $\alpha = 0$ and $\alpha = 1$ when the system is initialized with $|T_+\rangle$ and $|T_-\rangle$ states in the site $j = 1$. Specifically, (a) $|T_+\rangle$, $\alpha = 0$; (b) $|T_+\rangle$, $\alpha = 1$; (c) $|T_-\rangle$, $\alpha = 0$; and (d) $|T_-\rangle$, $\alpha = 1$. On the top of each panel, we report the SN dynamics of the Lth site density matrix.

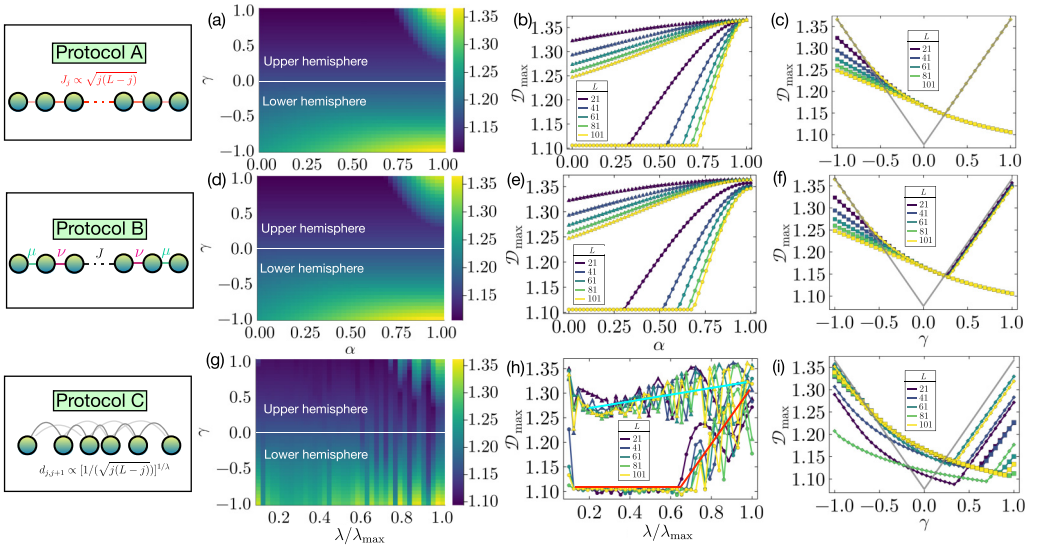


FIG. 3. Maximum transferable SN in the three protocols. Panels (a)–(c) show results for Protocol A (schematically illustrated on the left). Panel (a) reports the maximum transferable SN, $\mathcal{D}_{\max}$, as a function of the Hamiltonian parameter α and the initial-state parameter γ for $L = 101$. Panel (b) shows $\mathcal{D}_{\max}$ vs α for different system sizes L, comparing two initial states: $\gamma = -1$ ($|T_-\rangle$, triangles) and $\gamma = 1$ ($|T_+\rangle$, circles). Panel (c) displays $\mathcal{D}_{\max}$ as a function of γ for different values of L, with squares denoting $\alpha = 0$ and diamonds denoting $\alpha = 1$ (PST). The gray curve indicates the SN of the first site initial state. In the PST case, for $\gamma < \gamma_*$, $\mathcal{D}_{\max}(\gamma) = 0.073\,25(12)\,\exp[-1.3101(16)\,\gamma] + 1.093\,23(11)$, while for $\gamma > \gamma_*$, $\mathcal{D}_{\max}(\gamma) \simeq \frac{1}{2}(1 + \frac{2}{\sqrt{3}}) + \frac{\gamma}{2\sqrt{3}}$, with $\gamma_* \simeq 0.239$ estimated from the intersection of the two asymptotic expressions. The fit curve for $\gamma < \gamma_*$ normalized to the maximum possible stabilizer norm $\mathcal{D}_{\max}(\gamma = \pm 1) \simeq 1.366$ gives, up to the fit uncertainties, $\frac{\mathcal{D}_{\max}(\gamma)}{\mathcal{D}_{\max}(\gamma=\pm 1)} \simeq [0.0536e^{-1.3101\gamma} + 0.8003]$. Panels (d)–(i) show the analogous results for Protocol B and Protocol C, respectively. In the latter case, the horizontal axis is rescaled as $\lambda/\lambda_{\max}$, with $\lambda_{\max} = 5$ denoting the largest value considered; $\lambda/\lambda_{\max} = 1$ corresponds to the point closest to the PST regime explored in our simulations. In panel (h), the cyan and red curves serve as guides to the eye, respectively, the $\gamma = -1$ and $\gamma = 1$ behaviors. In panel (i), squares denote $\lambda = 0.1$ and diamonds $\lambda = \lambda_{\max} = 5$.

observation window to $T = N\tau_{\text{ref}}$, with $N = 10$ chosen to ensure that several reflection periods are included in the analysis. For a fixed protocol, $\rho^{(L)}(t)$ depends on the parameter α and on the choice of the single-qubit state encoded at the initial time $t = 0$. The previous section examined magic transfer for the two states $|T_+\rangle$ and $|T_-\rangle$. Here, we extend the analysis by studying the maximum transferable stabilizer norm for input states that are, in general, mixed, of the form $\rho_\gamma^{(1)}(0) = \frac{1}{2}(\hat{\mathbb{I}} + \frac{1}{\sqrt{3}}\hat{\sigma}_1^x + \frac{1}{\sqrt{3}}\hat{\sigma}_1^y + \frac{\gamma}{\sqrt{3}}\hat{\sigma}_1^z)$, with $\gamma \in [-1, 1]$ interpolating between $|T_-\rangle$ and $|T_+\rangle$. Thus, $\mathcal{D}_{\max} = \mathcal{D}_{\max}(\alpha, \gamma)$ exhibiting nontrivial features in the parameter space (α, γ) [(λ, γ) in the case of protocol C].

Our results are summarized in Fig. 3 for the three aforementioned protocols [51]. We first observe that the maximum transferable SN depends nontrivially on both the initial state preparation (γ) and the Hamiltonian configuration (α) across all three protocols [Figs. 3(a), 3(d), and 3(g)]. States initialized in the upper hemisphere exhibit a clear crossover behavior characterized by a threshold α_* that must be exceeded to achieve high-quality magic transfer. Conversely, for initial states in the lower hemisphere, $\mathcal{D}_{\max}$ displays smooth behavior. Physically, this means that in the first case the system starts in a down-spin state at the last site, so a threshold must be overcome before the coupling to neighboring spins displaces the Bloch vector sufficiently far from the stabilizer polytope, enabling efficient transfer of magic. In addition, we observe a common behavior across all three protocols, with Protocol C exhibiting more erratic behavior, consistent with prior work

on the effects of long-range interactions on perfect state transfer [53]. As the ballistic scheme (Protocol B) provides speed advantages over the transfer times required for PST [4,54], this appears to be indicative of the existence of an explicit class of quantum states capable of propagating through the system more rapidly without being taxed by as substantial a reduction in the faithfulness of the transport.

The presence of the threshold α_* for initial $|T_+\rangle$ states can be better appreciated in Figs. 3(b), 3(e), and 3(h), where $\mathcal{D}_{\max}(\alpha)$ is reported for different system sizes L for both $|T_+\rangle$ and $|T_-\rangle$. We observe that Protocols A and B share approximately the same threshold location, with the latter increasing with L, suggesting high-quality transfer only in the $\alpha \to 1$ limit as $L \to \infty$. Protocol C instead exhibits a more erratic behavior, with no clear size dependence of the threshold. In any case, we find $\lambda_* \gtrsim 3$, suggesting that relevant magic transfer emerges only when long-range effects become sufficiently suppressed.

Finally, in Figs. 3(c), 3(f), and 3(i), we report $\mathcal{D}_{\max}(\gamma)$ for different system sizes at fixed $\alpha = 0$ and $\alpha = 1$ (PST) for Protocols A and B, and at $\lambda = 0.1$ and $\lambda = 5$ for Protocol C. Tuning $\gamma \in [-1, 1]$ corresponds to moving from the lower to the upper hemisphere. The quantity $\mathcal{D}_{\max}(\gamma)$ is compared with $\mathcal{D}(\rho^{(1)}(0))$, shown in gray. For Protocols A and B, we observe a clear distinction between the noisy and PST (or QPST) regimes. In the former, $\mathcal{D}_{\max}$ decreases monotonically with γ and shows a strong system-size dependence in the lower hemisphere, confirming that the upper hemisphere corresponds to low-quality magic transfer. In contrast, the PST (and QPST) regime behaves markedly differently: $\mathcal{D}_{\max}(\gamma)$ is well described by an exponentially decaying branch separated by a crossover point $\gamma_* \simeq 0.239$ from a linearly increasing branch. In this regime, $\mathcal{D}_{\max}$ follows the same behavior as the initial state, indicating that the maximum transferable stabilizer norm coincides with that of the injected state. Here, the dependence on system size is absent or negligible. We also identify a region of γ in the central part of the Bloch sphere where the maximum transferable SN exceeds that of the initial state, indicating a form of magic enhancement associated with the state being driven deep into the nonstabilizer region, far from the stabilizer polytope. For Protocol C, we do not observe a clear L dependence. The separation between the monotonically decreasing and linearly increasing regimes, marked by a crossover point, persists for both values of λ considered.

Finally, we mention that these behaviors persist for $|H\rangle$ states [51], the other fundamental class of magic states for universal quantum computation [17], suggesting that they are not specific to a particular magic-state family, but instead reflect more general features of the dynamics and the structure of the protocol.

Conclusions and outlook. In this work, we investigated the transport of quantum magic through spin chain quantum buses, quantifying the transferred resource via the stabilizer norm. To probe genuinely nontrivial transport regimes, we focused on buses whose dynamics do not, in general, coincide with those supporting PST or QPST, except for specific parameter choices. In particular, we analyzed two Protocols, A and B, controlled by a parameter α that interpolates between homogeneous couplings and PST/QPST-supporting configurations, together with a third protocol, C, motivated by experimentally realizable trapped-ion architectures.

We find that magic transport is strongly influenced by the geometry of the initial state on the Bloch sphere. While magic encoded in states belonging to the lower hemisphere is efficiently transferred across a broad parameter range, states in the upper hemisphere exhibit a transport threshold in α, below which magic transfer is strongly suppressed. This reveals a marked asymmetry in the transport properties of quantum magic that is absent in conventional state-transfer figures of merit. This asymmetry is particularly evident for T states. Upper-hemisphere T states exhibit transport thresholds that increase with the size of the system, requiring progressively finer tuning and eventually approaching regimes compatible with PST/QPST. In contrast, lower-hemisphere T states do not show threshold behavior and present a larger maximum transferable stabilizer norm.

Furthermore, for nonmaximally magic input states, the conditions maximizing state-transfer fidelity do not generally coincide with those maximizing the transported magic. More strikingly,

we identify a parameter regime in which the quantum bus not only transfers but also amplifies the injected magic, yielding a stabilizer norm at the receiving end larger than that of the initially encoded state. These results establish a distinct resource-transfer problem beyond conventional PST-based paradigms and demonstrate that experimentally relevant spin-chain architectures can also exhibit nontrivial quantum-magic transport capabilities.

Future work may address the effects of disorder, finite temperature, dissipation, multiple-excitation subspaces, and repeated bus operation on the transport and enhancement of quantum magic. Understanding these effects is also essential from an experimental perspective, where the transfer of nonstabilizer resources may be realized in superconducting circuits [16,55], photonic platforms [13], trapped-ion systems [47,52], and atomtronic networks [56], enabling the distribution of quantum computational resources across quantum spin networks. Furthermore, interfacing these protocols with quantum-error-correction schemes and extending them to logical qubits represents an important and promising direction for future research.

Acknowledgments. A.P. and F.P. acknowledge O. La Rocca for valuable discussions during the development of this work. A.P. and F.P. acknowledge support from PNRR MUR Project No. PE0000023-NQSTI through the secondary project ThAnQ. C.N. acknowledges support from Engineering and Physical Sciences Research Council (EPSRC), Grant No. EP/W524657/1. E.C.D. acknowledges support from the European Union's Horizon Europe research and innovation programme under Grant Agreement No. 101114305 (MILLENION-SGA1 EU Project), from PID2021-127726NB-I00 and PID2024-161474NB-I00 (MCIU/AEI/FEDER,UE), and from QUITEMAD-CM TEC-2024/COM-84. E.C.D. also acknowledges support from the Grant IFT Centro de Excelencia Severo Ochoa CEX2020-001007-S funded by MCIN/AEI/10.13039/501100011033, and from the CSIC Research Platform on Quantum Technologies PTI-001.

Data availability. There are no publicly available research data or software supporting this manuscript. Requests for further information or data should be sent to the authors.

[1] S. Bose, Quantum communication through an unmodulated spin chain, Phys. Rev. Lett. **91**, 207901 (2003).

[2] M. Christandl, N. Datta, A. Ekert, and A. J. Landahl, Perfect state transfer in quantum spin networks, Phys. Rev. Lett. **92**, 187902 (2004).

[3] L. Vinet and A. Zhedanov, How to construct spin chains with perfect state transfer, Phys. Rev. A **85**, 012323 (2012).

[4] T. J. G. Apollaro, L. Banchi, A. Cuccoli, R. Vaia, and P. Verrucchi, 99%-fidelity ballistic quantum-state transfer through long uniform channels, Phys. Rev. A **85**, 052319 (2012).

[5] S. Ahuja, T. K. Konar, L. G. C. Lakkaraju, and A. Sen(De), Expediting quantum state transfer through the long-range extended XY model, Phys. Rev. A **113**, 022426 (2026).

[6] M. Christandl, L. Vinet, and A. Zhedanov, Analytic next-to-nearest-neighbor XX models with perfect state transfer and fractional revival, Phys. Rev. A **96**, 032335 (2017).

[7] F. Bezaz, C. C. Nelmes, M. P. Estarellas, T. P. Spiller, and I. D'Amico, Quasi-perfect state transfer in spin chains via parametrization of on-site energies, Phys. Scr. **100**, 055114 (2025).

[8] D. Murphy, A. Kiely, I. D'Amico, and S. Campbell, Ergotropy transport in a one-dimensional spin chain, Phys. Rev. A **112**, 052214 (2025).

[9] G. De Chiara, D. Rossini, S. Montangero, and R. Fazio, From perfect to fractal transmission in spin chains, Phys. Rev. A **72**, 012323 (2005).

[10] W. J. Chetcuti, C. Sanavio, S. Lorenzo, and T. J. G. Apollaro, Perturbative many-body transfer, New J. Phys. **22**, 033030 (2020).

[11] O. Michel, M. Werner, and A. Riera, A quantum state transfer protocol with Ising Hamiltonians, Quantum Sci. Technol. **11**, 035006 (2026).
[12] S. Campbell, T. J. G. Apollaro, C. Di Franco, L. Banchi, A. Cuccoli, R. Vaia, F. Plastina, and M. Paternostro, Propagation of nonclassical correlations across a quantum spin chain, Phys. Rev. A **84**, 052316 (2011).
[13] R. J. Chapman, M. Santandrea, Z. Huang, G. Corrielli, A. Crespi, M.-H. Yung, R. Osellame, and A. Peruzzo, Experimental perfect state transfer of an entangled photonic qubit, Nat. Commun. **7**, 11339 (2016).
[14] L. Xiang, J. Chen, Z. Zhu, Z. Song, Z. Bao, X. Zhu, F. Jin, K. Wang, S. Xu, Y. Zou, H. Li, Z. Wang, C. Song, A. Yue, J. Partridge, Q. Guo, R. Mondaini, H. Wang, and R. T. Scalettar, Enhanced quantum state transfer by circumventing quantum chaotic behavior, Nat. Commun. **15**, 4918 (2024).
[15] B. Li, Y. Cao, Y.-H. Li, W.-Q. Cai, W.-Y. Liu, J.-G. Ren, S.-K. Liao, H.-N. Wu, S.-L. Li, L. Li, N.-L. Liu, C.-Y. Lu, J. Yin, Y.-A. Chen, C.-Z. Peng, and J.-W. Pan, Quantum state transfer over 1200 km assisted by prior distributed entanglement, Phys. Rev. Lett. **128**, 170501 (2022).
[16] L. Zhou, Q. Xu, T. Feng, and X. Zhou, Experimental realization of a three-photon asymmetric maximally entangled state and its application to quantum state transfer, Sci. Adv. **10**, eadj9251 (2024).
[17] S. Bravyi and A. Kitaev, Universal quantum computation with ideal Clifford gates and noisy ancillas, Phys. Rev. A **71**, 022316 (2005).
[18] E. T. Campbell, Catalysis and activation of magic states in fault-tolerant architectures, Phys. Rev. A **83**, 032317 (2011).
[19] M. Howard and E. Campbell, Application of a resource theory for magic states to fault-tolerant quantum computing, Phys. Rev. Lett. **118**, 090501 (2017).
[20] K. Warmuz, E. Dokudowiec, C. Radhakrishnan, and T. Byrnes, Magic monotone for faithful detection of nonstabilizerness in mixed states, Phys. Rev. Lett. **135**, 010203 (2025).
[21] T. Haug and L. Piroli, Stabilizer entropies and nonstabilizerness monotones, Quantum **7**, 1092 (2023).
[22] V. Veitch, S. A. Hamed Mousavian, D. Gottesman, and J. Emerson, The resource theory of stabilizer quantum computation, New J. Phys. **16**, 013009 (2014).
[23] M. Sarkar, R. Ghosh, C. G. Smith, M. Myronov, and S. Bose, All-electric quantum state transfer via spin-orbit phase matching, arXiv:2605.13976.
[24] L. Leone, S. F. E. Oliviero, and A. Hamma, Stabilizer Rényi entropy, Phys. Rev. Lett. **128**, 050402 (2022).
[25] S. F. E. Oliviero, L. Leone, A. Hamma, and S. Lloyd, Measuring magic on a quantum processor, npj Quantum Inf. **8**, 148 (2022).
[26] T. Haug and L. Piroli, Quantifying nonstabilizerness of matrix product states, Phys. Rev. B **107**, 035148 (2023).
[27] P. S. Tarabunga, E. Tirrito, T. Chanda, and M. Dalmonte, Many-body magic via Pauli-Markov chains—From criticality to gauge theories, PRX Quantum **4**, 040317 (2023).
[28] E. Tirrito, P. S. Tarabunga, G. Lami, T. Chanda, L. Leone, S. F. E. Oliviero, M. Dalmonte, M. Collura, and A. Hamma, Quantifying nonstabilizerness through entanglement spectrum flatness, Phys. Rev. A **109**, L040401 (2024).
[29] T. Haug and P. S. Tarabunga, Efficient witnessing and testing of magic in mixed quantum states, npj Quantum Inf. **12**, 40 (2026).
[30] G. Passarelli, R. Fazio, and P. Lucignano, Nonstabilizerness of permutationally invariant systems, Phys. Rev. A **110**, 022436 (2024).
[31] T. Haug, L. Aolita, and M. Kim, Probing quantum complexity via universal saturation of stabilizer entropies, Quantum **9**, 1801 (2025).
[32] E. Tirrito, P. S. Tarabunga, D. S. Bhakuni, M. Dalmonte, P. Sierant, and X. Turkeshi, Universal spreading of nonstabilizerness and quantum transport, arXiv:2506.12133.
[33] H. Timsina, Y.-M. Ding, E. Tirrito, P. S. Tarabunga, B.-B. Mao, M. Collura, Z. Yan, and M. Dalmonte, Robustness of nonstabilizerness in the quantum Ising chain via quantum Monte Carlo tomography, Phys. Rev. B **112**, 165135 (2025).

[34] X. Turkeshi, E. Tirrito, and P. Sierant, Magic spreading in random quantum circuits, Nat. Commun. **16**, 2575 (2025).
[35] M. Viscardi, M. Dalmonte, A. Hamma, and E. Tirrito, Interplay of entanglement structures and stabilizer entropy in spin models, SciPost Phys. Core **9**, 012 (2026).
[36] G. Passarelli, P. Lucignano, D. Rossini, and A. Russomanno, Chaos and magic in the dissipative quantum kicked top, Quantum **9**, 1653 (2025).
[37] A. Russomanno, G. Passarelli, D. Rossini, and P. Lucignano, Nonstabilizerness in the unitary and monitored quantum dynamics of XXZ-staggered and Sachdev-Ye-Kitaev models, Phys. Rev. B **112**, 064312 (2025).
[38] A. Scocco, W.-K. Mok, L. Aolita, M. Collura, and T. Haug, Rise and fall of nonstabilizerness via random measurements, Phys. Rev. Res. **8**, 013217 (2026).
[39] J. Odavić, T. Haug, G. Torre, A. Hamma, F. Franchini, and S. M. Giampaolo, Complexity of frustration: A new source of non-local non-stabilizerness, SciPost Phys. **15**, 131 (2023).
[40] R. Smith, Z. Papić, and A. Hallam, Nonstabilizerness in kinetically constrained Rydberg atom arrays, Phys. Rev. B **111**, 245148 (2025).
[41] S. Sarkar, G. Biswas, J.-Y. Wu, and A. Biswas, Reduced-state stabilizer Rényi entropy as a probe of quantum criticality in the transverse ANNNI model and the quantum compass model, arXiv:2605.18391.
[42] E. Zavatti, G. Bellomia, and M. Capone, Quantum magic of strongly correlated fermions—The Hubbard dimer, arXiv:2605.18494.
[43] P. Martinez-Azcona, M. Sarkis, A. Tkatchenko, and A. Chenu, Magic steady state production: Non-Hermitian, dissipative, and stochastic pathways, Quantum Sci. Technol. **11**, 045083 (2026).
[44] A. Grabarits and A. del Campo, Universal non-stabilizerness dynamics across quantum phase transitions, arXiv:2603.08841.
[45] J. Franke, S. R. Muleady, R. Kaubruegger, F. Kranzl, R. Blatt, A. M. Rey, M. K. Joshi, and C. F. Roos, Quantum-enhanced sensing on optical transitions through finite-range interactions, Nature (London) **621**, 740 (2023).
[46] N. Defenu, T. Donner, T. Macrì, G. Pagano, S. Ruffo, and A. Trombettoni, Long-range interacting quantum systems, Rev. Mod. Phys. **95**, 035002 (2023).
[47] M. Foss-Feig, G. Pagano, A. C. Potter, and N. Y. Yao, Progress in trapped-ion quantum simulation, Annu. Rev. Condens. Matter Phys. **16**, 145 (2025).
[48] A. Browaeys and T. Lahaye, Many-body physics with individually controlled Rydberg atoms, Nat. Phys. **16**, 132 (2020).
[49] D. Barredo, H. Labuhn, S. Ravets, T. Lahaye, A. Browaeys, and C. S. Adams, Coherent excitation transfer in a spin chain of three Rydberg atoms, Phys. Rev. Lett. **114**, 113002 (2015).
[50] L. Leone and L. Bittel, Stabilizer entropies are monotones for magic-state resource theory, Phys. Rev. A **110**, L040403 (2024).
[51] See Supplemental Material at http://link.aps.org/supplemental/10.1103/mq4t-pnby for derivation of time evolution of local Bloch vectors, average fidelity and chain parameterization, stabilizer norm of the $|H\rangle$ state, and geometric representation of magic transport.
[52] D. Lewis, L. Banchi, Y. Hong Teoh, R. Islam, and S. Bose, Ion trap long-range XY model for quantum state transfer and optimal spatial search, Quantum Sci. Technol. **8**, 035025 (2023).
[53] R. Ronke, T. P. Spiller, and I. D'Amico, Effect of perturbations on information transfer in spin chains, Phys. Rev. A **83**, 012325 (2011).
[54] M.-H. Yung, Quantum speed limit for perfect state transfer in one dimension, Phys. Rev. A **74**, 030303(R) (2006).
[55] X. Li, Y. Ma, J. Han, T. Chen, Y. Xu, W. Cai, H. Wang, Y. Song, Z.-Y. Xue, Z.-Q. Yin, and L. Sun, Perfect quantum state transfer in a superconducting qubit chain with parametrically tunable couplings, Phys. Rev. Appl. **10**, 054009 (2018).
[56] J. Polo, W. J. Chetcuti, E. C. Domanti, P. Kitson, A. Osterloh, F. Perciavalle, V. P. Singh, and L. Amico, Perspective on new implementations of atomtronic circuits, Quantum Sci. Technol. **9**, 030501 (2024).